Nucleic Acids Research, 2024, **52**, 6964–6976
https://doi.org/10.1093/nar/gkad1222
Advance access publication date: 24 December 2023
Genome integrity, repair and replication

The BRCA2 R2645G variant increases DNA binding and induces hyper-recombination

Lucia Alvaro-Aranda[1,†], Ambre Petitalot[2,3,†], Yasmina Djeghmoum[4,5,†], Davide Panigada[4,5,†], Jenny Kaur Singh[4,5], Åsa Ehlén[4,5], Domagoj Vugic[4,5], Charlotte Martin[4,5], Simona Miron[6], Aida Contreras-Perez[1], Naima Nhiri[7], Virginie Boucherit[4,5], Philippe Lafitte[2,3], Isaac Dumoulin[4,5], Francisco Quiles[8,9], Etienne Rouleau[2,3], Eric Jacquet[7], Lidia Feliubadaló[8,9], Jesús del Valle[8,9], Shyam K. Sharan[10], Dominique Stoppa-Lyonnet[2,11,12], Sophie Zinn-Justin[6], Conxi Lázaro[8,9], Sandrine M. Caputo[2,3] and Aura Carreira[1,4,5,*]

[1]Genome Instability and Cancer Predisposition Laboratory, Centro de Biologia Molecular Severo Ochoa (CBMSO), CSIC-UAM, Madrid 28049, Spain
[2]Department of Genetics, Institut Curie, Paris 75005, France
[3]PSL Research University, Paris 75005, France
[4]Institut Curie, PSL Research University, CNRS, UMR3348, F-91405 Orsay, France
[5]Paris-Saclay University CNRS, UMR3348, F-91405 Orsay, France
[6]Institute for Integrative Biology of the Cell (I2BC), CEA, CNRS, Paris-Saclay University, 91190 Gif-sur-Yvette, France
[7]Institut de Chimie des Substances Naturelles, Paris-Saclay University, CNRS, 91190 Gif-sur-Yvette, France
[8]Hereditary Cancer Program, Catalan Institute of Oncology (ICO), Hereditary Cancer Group, Molecular Mechanisms and Experimental Therapy in Oncology Program, Institut d'Investigació Biomèdica de Bellvitge (IDIBELL), L'Hospitalet de Llobregat, Spain
[9]Ciber Oncología (CIBERONC), Instituto Salud Carlos III, Madrid, Spain
[10]Mouse Cancer Genetics Program, Center for Cancer Research, National Cancer Institute, Frederick, Maryland 21702, USA
[11]Paris-Cité University, Paris, France
[12]INSERM U830, Institut Curie, Paris 75005, France

[*]To whom correspondence should be addressed. Tel: +34 911964497; Email: acarreira@cbm.csic.es
[†]The first four authors should be regarded as Joint First Authors.

Abstract

BRCA2 tumor suppressor protein ensures genome integrity by mediating DNA repair via homologous recombination (HR). This function is executed in part by its canonical DNA binding domain located at the C-terminus ($BRCA2_{CTD}$), the only folded domain of the protein. Most germline pathogenic missense variants are located in this highly conserved region which binds to single-stranded DNA (ssDNA) and to the acidic protein DSS1. These interactions are essential for the HR function of BRCA2. Here, we report that the variant R2645G, identified in breast cancer and located at the DSS1 interface, unexpectedly increases the ssDNA binding activity of $BRCA2_{CTD}$ *in vitro*. Human cells expressing this variant display a hyper-recombination phenotype, chromosomal instability in the form of chromatid gaps when exposed to DNA damage, and increased PARP inhibitor sensitivity. In mouse embryonic stem cells (mES), this variant alters viability and confers sensitivity to cisplatin and Mitomycin C. These results suggest that BRCA2 interaction with ssDNA needs to be tightly regulated to limit HR and prevent chromosomal instability and we propose that this control mechanism involves DSS1. Given that several missense variants located within this region have been identified in breast cancer patients, these findings might have clinical implications for carriers.

Graphical abstract

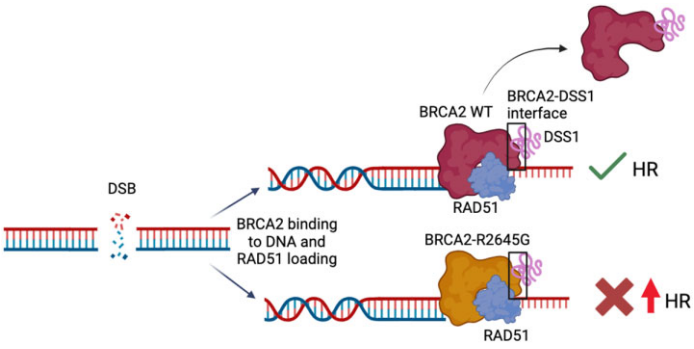

Received: August 8, 2023. **Revised:** November 30, 2023. **Editorial Decision:** December 10, 2023. **Accepted:** December 12, 2023

Introduction

Germline missense pathogenic variants affecting a single *BRCA2* allele predispose individuals to breast and ovarian cancer. BRCA2 is a multifunctional protein and exerts its main tumor-suppressive function in the cell nucleus through its role in DNA repair by homologous recombination (HR). In particular, it mediates the loading of the recombinase RAD51 on ssDNA preventing its assembly on dsDNA, and promoting the formation of an active RAD51 nucleoprotein filament for HR(1,2). Consequently, defects in this pathway perturb chromosome integrity (3).

BRCA2 is a large protein that is mainly disordered (4). It exhibits one single folded domain between amino acids 2478 and 3184 that binds to ssDNA, hereafter named $BRCA2_{CTD}$, and to the small acidic protein DSS1. Notably, most pathogenic missense variants have been identified in $BRCA2_{CTD}$ (5,6). Thus, studying this region and its interaction with DNA and DSS1 may shed light on the defective mechanisms that are linked to pathogenicity. DSS1 is required for the stability of BRCA2 (5,7,8) and plays important regulatory roles in the oligomerization of BRCA2 and BRCA2 binding to DNA (9–11). Moreover, DSS1 has been proposed to facilitate the displacement of RPA by RAD51 during HR by reducing the affinity of RPA for ssDNA (12).

In addition to the canonical $BRCA2_{CTD}$, BRCA2 contains DNA binding motifs in its disordered N-terminus (NTD) and within the C-terminal RAD51 binding region (13,14). BRCA2 oligomerizes through various interfaces that are not entirely characterized (10,15,16) and binding to DSS1 antagonizes this process (9,15). The interaction between BRCA2 and DSS1 also regulates BRCA2 localization in the cell due to a nuclear export signal (NES) that is occluded when DSS1 is bound to BRCA2. As such, several BRCA2 variants showing defective DSS1 binding are cytoplasmic, whereas overexpressing DSS1 enhances BRCA2 nuclear localization (15,17). Here, we report that BRCA2 R2645G, a variant affecting a residue located close to the DSS1 binding site, does not impair DSS1 binding but unexpectedly favors the interaction of $BRCA2_{CTD}$ with ssDNA *in vitro*. Human cells expressing BRCA2 with this variant exhibit a DNA double-strand break (DSB)- hyper-recombination phenotype as revealed in a gene targeting reporter assay (18) which results in chromosome instability and increased PARPi sensitivity. In addition, mouse embryonic stem cells bearing the same variant display reduced viability and increased sensitivity to MMC and cisplatin. Our results suggest that the interaction of BRCA2 with ssDNA needs to be tightly regulated to prevent excessive recombination. These findings might have clinical implications for carriers of this variant.

Materials and methods

Site-directed mutagenesis

Point mutations (R2520L, R2645G, R2659G) were introduced in $BRCA2_{CTD}$ (aa 2474–3190) or EGFP-MBP-BRCA2 vector using QuikChange II and QuikChange XL site-directed mutagenesis kit (Agilent Technologies), respectively, as previously described(28). Mutagenesis primers were designed using the QuickChange Primer Design program and purchased from MWG Eurofins. Mutations R2645G and G25R were introduced in the BAC CTD-2342K5 (generated by Dr Shyam Sharan's lab (23) and containing the whole human *BRCA2* gene), by recombineering using galK selection as previously described(34). All mutations were verified by Sanger sequencing.

Cell lines

The human cell lines HEK293-T cells (gift from Dr Mounira Amor-Gueret) were cultured in DMEM (Eurobio Abcys, Courtaboeuf, France) media containing 25 mM sodium bicarbonate and 2 mM L-glutamine supplemented with 10% FBS (EuroBio Abcys). The BRCA2 deficient colorectal adenocarcinoma cell line DLD1 $BRCA2^{-/-}$ (HD 105–007) was purchased from Horizon Discovery (Cambridge, England). The cells were cultured in RPMI media (EuroBio Abcys) containing 25 mM sodium bicarbonate and 2 mM L-Glutamine (EuroBio Abcys) supplemented with 10% FBS (EuroBio Abcys). The DLD1 $BRCA2^{-/-}$ cells were maintained in growth media containing 0.1 mg/ml hygromycin B (Thermo Fisher Scientific). The stable cell lines of DLD1 BRCA2 deficient cells expressing BRCA2 WT or variants of interest generated in this study were cultured in growth media containing 0.1 mg/ml hygromycin B (Thermo Fisher Scientific) and 1 mg/ml G418 (Sigma-Aldrich).

All cells were cultured at 37°C with 5% CO_2 in a humidified incubator and all cell lines used in this study have been regularly tested for mycoplasma contamination (MycoAlert, Lonza) and genotyped using GenePrint kit (Promega).

PL2F7 mouse embryonic stem cells used in the complementation and viability assays were generated by Dr Shyam Sharan's lab (23) have both *Brca2* alleles knocked out: one constitutive and one conditional ($Brca2^{ko/cko}$) and are deficient in *Hprt*.

Stable cell line generation

To generate DLD1 $BRCA2^{-/-}$ stable cell lines expressing human BRCA2 variants of interest we transfected one 100 mm plate of DLD1 $BRCA2^{-/-}$ cells at 70% of confluence with 10 μg of a plasmid containing human EGFP-MBP-tagged BRCA2 cDNA (carrying the mutation of interest) using TurboFect (Thermo Fisher Scientific) according to manufacturer's instructions; 48 h post-transfection the cells were serial diluted and cultured in media containing 0.1 mg/ml hygromycin B (Thermo Fisher Scientific) and 1 mg/ml G418 (Sigma-Aldrich) for selection. Single-cell colonies were isolated and later expanded and their genomic DNA was extracted to verify the mutation by sequencing. BRCA2 protein levels were detected by Western Blot using BRCA2 antibody (1:1000, OP95, EMD Millipore).

Protein expression and purification

CTD and the mutated forms were co-expressed with DSS1 to ensure the stability of the protein as previously described. *E. coli* BL21 DE3 cells were transformed and grown at 37°C in 7 l of Terrific Broth and induced with 0.5% arabinose and 1 mM IPTG overnight at optical density 2. The cells were collected in 20 mM Tris–HCl pH 8300 mM NaCl, 10% glycerol, 0.5 mM EDTA, 5 mM β-mercaptoethanol, 1× Protease Inhibitor Cocktail EDTA-free (Roche), 10 mM $MgCl_2$, 1× DNase, 0.5 mg/ml Lysozyme (Sigma-Aldrich) and the suspension was lysed by disintegration at 1.7 kbar. The His-tagged protein was incubated with Protino Ni-NTA agarose (Macherey Nagel) and eluted with 200 mM imidazole. After dialysis overnight against 20 mM Tris–HCl pH

8, 100 mM NaCl, 10% glycerol, 0.5 mM EDTA, 5 mM β-mercaptoethanol, the eluate was loaded onto a 5 ml HiTrap Heparin HP column (GE) and eluted using a continuous NaCl gradient (100–1 M NaCl) in the same buffer. When required, the pool of purified protein was reloaded into Protrino Ni-NTA agarose as above. The pool of nuclease-free fractions was dialyzed against a storage buffer containing 20 mM Tris–HCl pH 8, 100 mM NaCl, 10% glycerol, 0.5 mM EDTA and 5 mM β-mercaptoethanol. The protein concentration was determined by NanoDrop 2000 spectrophotometer (Fisher Scientific) and corrected for the contaminants bands by running the protein on a 10% acrylamide SDS PAGE gel and measured by ImageJ software.

His-DSS1 was expressed in the pET-M13 vector and produced in *Escherichia coli* BL21 (DE3) Star cells. The DSS1 protein expression was induced with 1 mM IPTG at an OD_{600} of 0.8 and further incubation of cells for 3h at 37°C. After centrifugation (at 3500 RPM, during 20 min, at 4°C) the cell pellets were resuspended in the lysis buffer (20 mM Tris–HCl, pH 7.5, NaCl 150 mM, 10 mM imidazole) with a 1× of EDTA-free Protease Inhibitor Cocktail (Roche) and disrupted by sonication. The cell lysate was treated with benzonase nuclease and $MgCl_2$ (5 mM) for 30 min at 4°C and then centrifugated (20 000 RPM) for 20 min at 4°C. The supernatant was filtrated (0.44 μm) and loaded at 1 ml/min on a HisTrap HP 5 ml column (GE Healthcare) which was equilibrated with buffer A (20 mM Tris–HCl, pH 7.5, NaCl 150 mM, 10 mM imidazole). The proteins were eluted with a linear gradient of imidazole from 0 to 100% of buffer B (20 mM Tris–HCl, pH 7.5, NaCl 150 mM, 400 mM imidazole). The purest fractions were pooled and were dialyzed (3.5 kDa) against 20 mM Tris–HCl, pH 7.5, and 150 mM NaCl buffer. The sample was concentrated on an Amicon Ultra Centrifugal Filter Unit (3 kDa cut-off) and injected at 1 ml/min on a HiLoad 10/300 Superdex 75 column (GE Healthcare) equilibrated in 20 mM Tris–HCl, pH 7.5, 150 mM NaCl. The purified protein was analyzed by SDS-PAGE and the concentration was estimated by spectrophotometric measurement of absorbance at 280 nm.

Thermostability measurements by fluorescence-based thermal shift assay (FBTSA)

The FBTSA method was used to monitor the CTD domain thermal denaturation and changes induced by a mutation and/ or a binding event. To measure the thermostability of WT and mutated CTD domain, we mixed 1.5 μg of purified protein in 20 mM Tris–HCl pH 8.0, 150 mM NaCl, 0.5 mM EDTA, 10% glycerol, 5 mM β-mercaptoethanol, and the SYPRO Orange dye (diluted 800-fold from a 5000-fold stock solution, Invitrogen) in a final volume of 20 μl. Each experiment was repeated at least twice, independently. Experiments were carried out in QuantStudio 12KFlex qPCR machine (Applied Biosystems) with a temperature gradient in the range of 10–95°C at 3°C/min. The fluorescence profiles, derivatives, and Tm were determined using the analysis software of the manufacturer.

Electrophoretic mobility shift assay

DNA substrates for EMSA were purchased PAGE-purified from MWG Eurofins. The ssDNA substrate used in EMSA was PAGE purified oAC423 ^{32}P-labelled at the 5′-end and contained the following sequence: 5′-CTGCTTTATCAAGATA ATTTTTCGACTCATCAGAAATATCCGTTTCCTATATTT ATTCCTATTATGTTTTATTCATTTACTTATTCTTTATG TTCATTTTTTATATCCTTTACTTTATTTTCTCTGTTTA TTCATTTACTTATTTTGTATTATCCTTATCTTATTTA-3′. The proteins were incubated at the indicated concentrations with 2 nM ssDNA ^{32}P-labelled DNA substrate for 5 min at 37°C in EMSA reaction buffer (25 mM Tris acetate pH 7.5, 1 mM DTT, 1 mM $MgCl_2$). For Figure 3B, $BRCA2_{CTD}$ and DSS1 were incubated for 15 min at 37°C before the incubation with DNA as above. The protein–DNA complexes were resolved on 6% native polyacrylamide gels in 1× TAE buffer (40 mM Tris acetate, 0.5 mM EDTA) at 70 V for 60 min at 4°C. The gels were dried and analyzed with a Typhoon PhosphorImager (Amersham Biosciences) using Image Quant software (GE Healthcare). In all EMSAs, the ratio of DNA–protein complexes was calculated as the percentage of bound DNA compared with the free DNA on each lane.

Subcellular fractionation

DLD1 stable clones expressing EGFP-MBP-BRCA2 WT, R2520L, R2645G or R2659G pellets were resuspended in BADT buffer (10 mM HEPES pH 7.9, 10 mM KCl, 10% glycerol, 1.5 mM $MgCl_2$, 0.34 M sucrose, Triton X-100 0.1%) supplemented with 1 × protease inhibitor cocktail (Complete, EDTA-free; Roche), 1 mM PMSF, 1 mM DTT, and 0.1 mM Na_3VO_4. The cell suspension was incubated for 20 min on ice and the cytoplasmic fraction was separated by centrifugation (supernatant). After a wash with BAD buffer (same as BADT buffer, without Triton X-100), the pellet was resuspended in 1x sample buffer, incubated on ice for 5 min, and sonicated. The two protein fractions were boiled for 5 min, separated by SDS–PAGE, and analyzed by Western blotting using anti-tubulin as a control for the cytoplasmic fraction. For all western blots, the protein bands were visualized with a ChemiDoc XRS+ System (BioRad). Stain-free images of the gels before transfer were used as loading control, and the cropped image is shown in the figure.

GFP-trap

GFP-pulldowns were performed on HEK293T cells transiently transfected with EGFP-MBP-NLS, EGFP-MBP-BRCA2 (WT or the VUS R2645G) and MBP-BRCA2-WT-RFP. Cells were lysed 36–48 h later in Co-IP lysis buffer (250 mM NaCl, 20 mM HEPES, 0.5% NP-40, 2 mM EGTA, 1.5 mM $MgCl_2$, 10% Glycerol, 1 mM DTT and 100 mM PMSF and protease inhibitor cocktail tablets) with or without 500 units benzonase, as indicated in the legends. Samples were incubated for 1 h at 4 °C under constant mixing. A 50 μg input sample was collected in a separate tube and mixed with 6x Laemmli buffer. The cleared lysates were subjected to GFP pull-down with GFP-Trap beads (Chromotek) for 2 h at 4°C. Around 3 mg of total protein, lysate was used per pull-down. The beads were then washed 5 times with Co-IP wash buffer (250 mM NaCl, 20 mM HEPES, 0.5% NP-40, 2 mM EGTA, 1.5 mM $MgCl_2$, 10% glycerol, 1 mM DTT and 100 mM PMSF and protease inhibitor cocktail tablets) and boiled for 5 min at 95°C in 3× Laemmli buffer along with the input samples. Proteins were separated by sodium dodecyl sulfate-polyacrylamide gel electrophoresis (SDS-PAGE) using 4–12% pre-cast polyacrylamide gels (Invitrogen) (Supplementary Figure S3B) or 4–15% precast polyacrylamide gels (BioRad) (Supplementary Figure S3A) and running buffer (1x Tris-Glycine, 0.1% SDS). The proteins were transferred for 2 h at 0.35 A at 4°C in nitro-

cellulose membranes. Membranes were scanned and analyzed using an Odyssey Infrared Imaging System (Licor; V3.0) and Image Studio Lite (version 5.2) (Supplementary Figure S3B) or developed using ECL prime western blotting detection reagent (VWR) and visualized using a ChemiDoc camera (BioRad) (Supplementary Figure S3A).

Antibodies used for western blotting

Primary antibodies used: mouse anti-BRCA2 (1:1000, OP95, EMD Millipore), mouse anti-αtubulin (1:5000, Cat. GTX628802 Genetex GT114, anti-DSS1 (1:500; sc-28848, Santa Cruz Biotechnology), anti-His (1:1000; Biolegend 9061019), rabbit anti-tRFP (1:1000, AB233, EVROGEN ENZO Life Sciences), mouse anti-GFP (1:1000, 11814460001, Sigma) Horseradish peroxidase (HRP)-conjugated secondary antibodies used were as follows: mouse anti-rabbit IgG-HRP (IB: 1:5000, Cat. sc-2357, Santa Cruz), and goat anti-mouse IgG-HRP (1:10000, Cat. # 115035-003, Interchim). For the Odyssey Infrared Imaging System (Licor; V3.0) secondary CF680 goat anti-rabbit or CF770 goat anti-mouse Ig antibodies (1:5000, Biotium) were used.

MTT viability test in human DLD1 cells

DLD1-derived cell lines were seeded in 96-well plates at different densities and treated 24 h later with different concentrations of PARP inhibitor (Olaparib AZD2281, Ku-0059436, Euromedex) (0, 0.5, 1, 2.5 μM). After 6 days of continuous treatment, cells were treated with 0.5μg/ml MTT (Thiazolyl Blue Tetrazolium Bromide; Sigma-Aldrich) diluted in culture medium, then incubated for 4h at 37°C, 5% CO_2 till the formation of blue crystals. Then the MTT was removed, and the crystals were dissolved in DMSO by shaking the plates for 10 min at RT following manufacturer specifications. The absorbance was measured in a plate reader (TriStar^2 LB 942, BERTHOLD scientific) at 570 nm. The survival percentage was calculated by dividing the absorbance into the cells treated by the absorbance obtained in cells left untreated.

BRCA2 complementation assay in mouse embryonic stem (mES) cells

Since *Brca2* is essential for the survival of mES cells, PL2F7 *Brca2*$^{ko/cko}$ mES cells were used to test the functional effect of *BRCA2* variants R2645G and G25R with a complementation assay(23): The *BRCA2* (mutated and WT) BACs were electroporated into the cells and selected with G418. *BRCA2* expression was analyzed by RT-PCR and six independent G418^r clones expressing *BRCA2* were electroporated with a Pgk-Cre345 plasmid. Thus, the conditional *Brca2* allele was depleted by the transient expression of Cre recombinase which, at the same time, restored the expression of an inserted *Hprt*, allowing its selection in the HAT medium. Forty-eight HAT^r colonies were analyzed by Southern blot to confirm the loss of the BRCA2^{cko} allele. HAT^r colonies were stained with methylene blue.

MTT viability test in mouse mES cells

To test the hypersensitivity of PL2F7 *Brca2*$^{ko/cko}$ mES cells transfected with *BRCA2* mutations R2645G and G25R, cells were seeded in triplicates and treated with the mitomycin C (MMC) or cisplatin at different concentrations as stated in the graphs in Figure 2C. Viability was measured with an MTT (3-(4,5-dimethylthiazol-2-yl)-2,5-diphenyl-2*H*-tetrazolium bromide) assay 72 h after treatment, as previously described (35).

Homologous recombination (HR) test

HR analysis was performed as previously described (18). Briefly, DLD1 cells were seeded one day before transfection at 1–3 × 10^6 cells/plate (depending on the cell line). Cells were co-transfected with TALENs to induce DNA double-strand break at the AAVS1 site in the PPP1R12C locus in the genome and a plasmid encoding a promoter-less mCherry fluorescent protein bearing 800 bp homologous sequences to the AAV1 site on each side. The transfection of 1 × 10^6 cells was performed using AMAXA Nucleofector™ 2b device following manufacturer specifications. Cells were then seeded in 6-well plates, maintained, and analyzed 8 days after transfection by flow cytometry. The percentage of mCherry positive cells was analyzed on a BD FACSAria III (BD Bioscience) using the FACSDiva software and data were analyzed with the FlowJo 10.5 software (Tree Star Inc.). Viable and single cells were gated using forward scatter (FSC-A) and side scatter (SSC-S). To separate single cells from the doublets, singlets were selected using FSC-W(y-axis) plotted against FSC-A(x-axis), mCherry positive cells were detected by plotting mCherry-A(y-axis) against FSC-A(x-axis).

Metaphase spreads

Around 1 × 10^5 and 2 × 10^5 cells depending on the cell line were seeded onto six-well plates on coverslips and treated with Mitomycin C (SIGMA M4287-2MG) (3 μM 1 h at 37°C) and the following day was arrested in metaphase by adding 0.1 μg/ml colcemid (Thermofisher 15212012) for 3 h at 37°C. A hypotonic shock was performed by incubating the cells with pre-warmed 16% FBS in water for 40 min. Following the hypotonic shock, the cells were fixed by adding 1 volume of methanol–acetic acid (3:1) into one volume of 16% FBS for 15 min at RT, then methanol: acetic acid (3:1) into one volume of water for 5 min at RT, then methanol–acetic acid (3:1) 30 min RT, and methanol–acetic acid (3:1) for 15 min 4 °C. DNA was stained with 2% Giemsa (Thermo Fisher 10092013) diluted in Gurr buffer (Thermo Fisher 10582013) for 16 min. Chromosomes were acquired either with a Leica DMRB microscope at ×100 magnification and captured with a SONY DXC 930P camera or with a Zeiss Axioskop 2 plus microscope at ×100 magnification and captured with a Leica DMC6200 camera. Chromosomal aberrations were manually counted using Fiji software. Around 50 metaphases were analyzed for cells of each genotype.

Statistical analysis

The total number of experimental replicates, mean, median, and error bars are described in the figure legends. Statistical difference was calculated using a two-way ANOVA test with Dunnett's multiple comparisons tests (Figures 2A, C, 4A) or Kruskal–Wallis test followed by Dunn's multiple comparison tests (Figure 4B and Supplementary Figure S5). A non-linear regression was used to fit the curves in Figure 3A and B and obtain apparent the dissociation constants shown in Table 2. All analyses were conducted using GraphPad Prism version Mac OS X 10.0.1 (170).

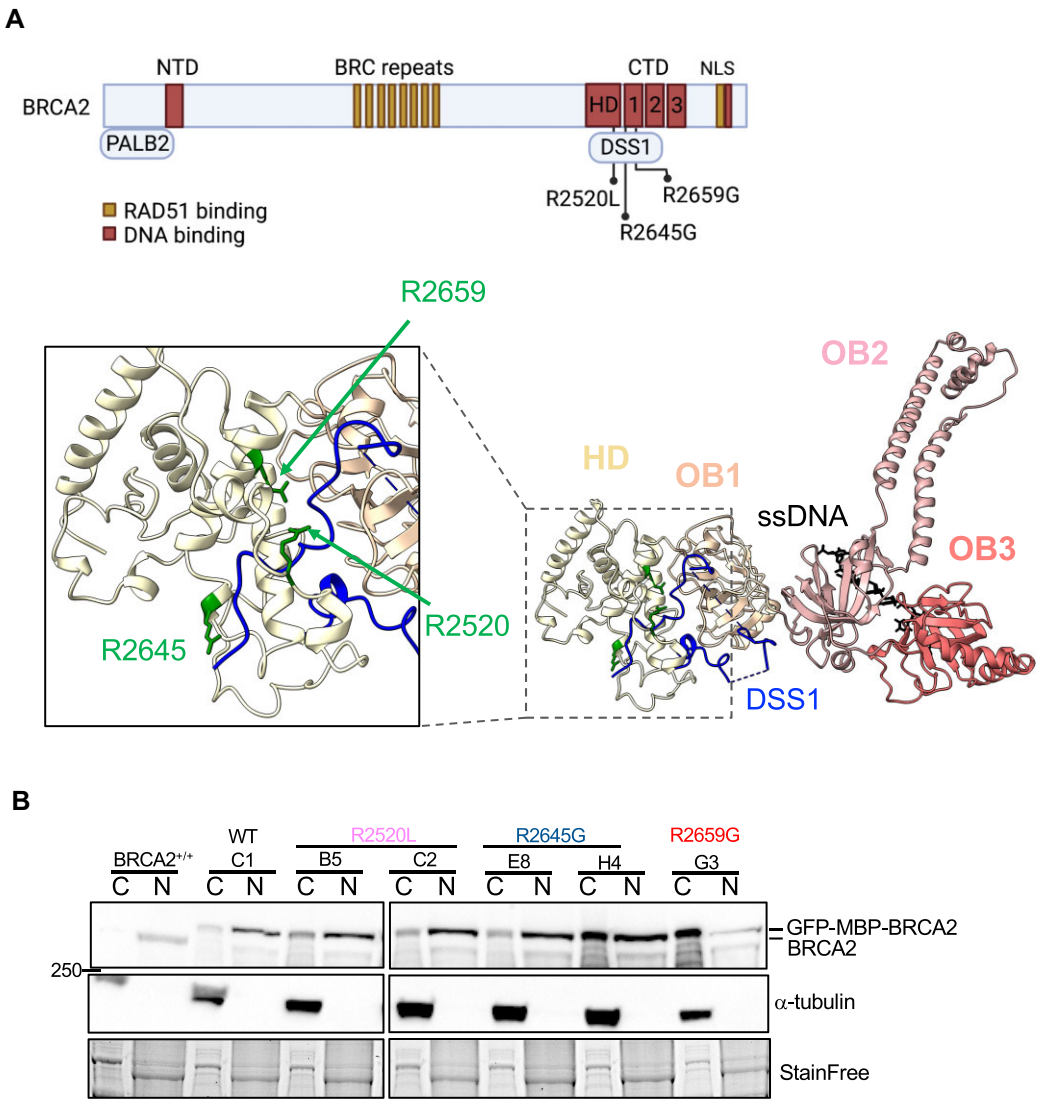

Figure 1. BRCA2 variants R2520L and R2645G at the DSS1 interface do not alter BRCA2 nuclear localization. (**A**) (Top) Scheme of BRCA2 showing its main functional domains and the selected VUS. Figure created with BioRender.com. (Bottom) Human model of $BRCA2_{CTD}$ based on mouse $Brca2_{CTD}$ (1MJE) showing the localization of the residues affected by the selected VUS (in green). In this model, $BRCA2_{CTD}$ (in white to dark pink) binds to DSS1 (in blue) and a ssDNA (in black). (**B**) Nuclear/cytoplasmic fractionation of stable clones bearing *BRCA2* VUS presented in (A).

Results

Variants R2520L and R2645G at the DSS1 interface do not alter BRCA2 nuclear localization

DSS1 and DNA have been reported as the main regulators of the oligomeric form of BRCA2 *in vitro* (10,16). Moreover, impairing DSS1 interaction as shown in several BRCA2 missense variants, affects the stability of the protein (5,8) and exposes a nuclear export signal (NES), which triggers the mislocalization of BRCA2 in the cytoplasm and abrogates its function (15,17). The negatively charged and disordered DSS1 has been previously hypothesized to mimic DNA, modulating accessibility of DNA binding sites in the BRCA2 Helical domain and OB1 (5). We set out to characterize BRCA2 missense variants identified in high-risk breast/ovarian cancer patients and predicted to impact DSS1 interaction to shed light on this regulation. We selected three variants of unknown clinical significance (VUS), R2520L (c.7559G > T), R2645G (c.7933A > G) and R2659G (c.7975A > G) affecting three highly conserved residues (Supplementary Figure S1), located within the helical domain at the interface with DSS1 (Figure 1A). Among them, R2659G has been recently classified as pathogenic and R2645G as likely benign(19), whereas R2520L remains a VUS.

We generated stable cell lines bearing the selected variants by transfecting the *BRCA2* cDNA coding for a GFP-MBP-tagged version of BRCA2 full-length protein (BRCA2 WT) as well as the variants R2520L, R2645G or R2659G in DLD1 BRCA2 deficient human cells (hereafter $BRCA2^{-/-}$). In this cell line, both alleles of BRCA2 contain a deletion in exon 11 leading to a premature stop codon after BRC5 and cytoplasmic localization of the truncated form of the protein (20). Wherever possible, we selected two stable clones of each variant to account for phenotypic differences that could be due to the variability in protein levels among the clones compared to the wildtype counterpart (clone C1, hereafter BRCA2 WT). We then conducted a nuclear/cytoplasmic fractionation and immunoblotted for BRCA2, α-tubulin serving as a cytoplasmic marker. As expected, the majority of

Table 1. Thermofluor-based analysis of the thermal stability of $BRCA2_{CTD}$ WT and mutated forms that were used in this study

Name	Tm ± SD	Replicates	Δ (MUT - WT)
$BRCA2_{CTD}$ WT	55.02 ± 0.13	21	0.00
$BRCA2_{CTD}$ R2520L	52.51 ± 0.20	13	−2.52
$BRCA2_{CTD}$ I2627F	47.90 ± 0.10	4	−7.12
$BRCA2_{CTD}$ R2645G	54.07 ± 0.20	6	−0.95
$BRCA2_{CTD}$ R2659G	ND	ND	ND
$BRCA2_{CTD}$ R3052W	49.87 ± 1.82	19	−5.15

Tm, melting temperature. ND, non-determined.

endogenous BRCA2 localized to the nucleus and this was also the case in the cells complemented with the BRCA2 WT clone (WT C1). The same pattern was observed with clones B5 and C2 of R2520L and H4 and E8 of R2645G. In contrast, cells expressing R2659G G3 displayed a strong cytoplasmic signal with strongly reduced levels of nuclear protein showing that this variant was largely mislocalized in cells (Figure 1B).

Taken together, we produced DLD1 BRCA2 deficient cells stably expressing GFP-MBP-BRCA2 with the variants R2520L, R2645G, and R2659G, and we observed that all except BRCA2 R2659G localized in the nucleus.

Variants R2520L and R2645G bind DSS1 but mildly destabilize $BRCA2_{CTD}$ *in vitro*

A large set of BRCA2 pathogenic mutations at the interface with DSS1 have previously been characterized for their impact on DSS1 binding and nuclear localization in cells (15). Among them, variants I2627F and R2659T in the HD domain, T2722R, D2723H and G2748D in the OB1 domain showed defective DSS1 binding whereas R3052W in the OB3 domain did not. However, all of these variants altered the nuclear localization of a construct expressing the C-terminal region of BRCA2 that comprised the folded $BRCA2_{CTD}$. To determine the impact of R2520L, R2645G and R2659G on BRCA2 molecular properties, we produced and purified a set of recombinant $BRCA2_{CTD}$ variants co-expressed with DSS1 in bacteria (13), including the 6 previously characterized and our three variants. We then measured their capacity to co-purify with DSS1 and assessed their thermal stability. In the control set of variants, $BRCA2_{CTD}$-R2659T, -T2722R, -D2723H and -G2748D could not be produced as soluble proteins when co-expressed with DSS1 in bacteria. $BRCA2_{CTD}$-I2627F and R3052W were poorly expressed, and their thermal stability was severely decreased (I2627F: 48°C; R3052W: 45.5–51.5°C (mean 49.9) compared to that of the WT domain (55°C)) (Table 1). Yet, they both co-eluted with DSS1 (Supplementary Figure S2A, B). In the case of our 3 variants, R2659G was very poorly expressed and could not be properly purified (Supplementary Figure S2A), whereas R2520L and R2645G were well-expressed, their thermal temperatures were mildly reduced (R2520L: 52°C; R2645G: 54°C (Table 1, Supplementary Figure S2C)) and they copurified with DSS1 (Supplementary Figure S2A, S2B).

Taken together, two of our variants, $BRCA2_{CTD}$-R2520L and -R2645G, copurified with DSS1, suggesting no impaired binding, and showed a mild decrease in thermal stability compared to $BRCA2_{CTD}$-WT. This contrasts with the control variants, $BRCA2_{CTD}$-R3052W and I2627F, which showed significantly lower thermal stability despite their co-elution with DSS1.

BRCA2 R2645G variant confers sensitivity to genotoxic agents

Poly (ADP-ribose) polymerase (PARP) inhibitors, in particular Olaparib, are currently used in the clinic to treat breast and ovarian cancer patients carrying germline (likely) pathogenic variants in *BRCA1/2* (21) as they are particularly toxic in HR-deficient cells(22). To assess the sensitivity to Olaparib of cells bearing the three variants, we performed an MTT assay. The relative viability of DLD1 BRCA2 deficient cells was ∼20% upon a 6-day treatment with the highest Olaparib concentration used (2.5 μM); in contrast, 80% of BRCA2 WT complemented cells remained viable, similar to the cells expressing the endogenous BRCA2 protein (Figure 2A). A similar trend was observed for the two clones expressing R2520L. In contrast, cells bearing R2659G, the variant that was found mainly in the cytoplasmic fraction (Figure 1B), showed as much sensitivity as the BRCA2 deficient cells. Interestingly, the two clones bearing R2645G displayed an intermediate phenotype.

To confirm the possible impact of the variant R2645G in a different cell system, we used mouse embryonic stem cells (mES) in which the selected variant was introduced by mutagenesis and recombination in a bacterial artificial chromosome (BAC) containing human BRCA2. In these cells, one endogenous allele of mBrca2 is defective whereas the other functional mBrca2 allele is conditionally removed by Cre-recombinase transient transfection (23). The ability of the mutated BRCA2 form to rescue the lethality of mBrca2 deficiency was then analyzed: BRCA2-R2645G conferred reduced viability in a colony formation assay as compared to the WT counterpart suggesting it partially alters BRCA2 function (Figure 2B). Moreover, mES expressing BRCA2-R2645G exhibited hypersensitivity to MMC and cisplatin, comparable to the control BRCA2-G25R, a variant previously shown to display sensitivity to DNA damaging agents and reduced HR (24) (Figure 2C).

Altogether, human DLD1 $BRCA2^{-/-}$ cells expressing BRCA2-R2659G showed hypersensitivity to PARPi whereas cells expressing BRCA2-R2520L did not. Cells bearing the variant BRCA2-R2645G exhibited an intermediate sensitivity to PARPi compared to BRCA2 WT complemented cells. In addition, mES cells expressing BRCA2-R2645G displayed compromised viability in a colony formation assay and showed sensitivity to MMC and cisplatin in the same cell system, suggesting a defect in BRCA2 function.

The BRCA2 R2645G variant enhances $BRCA2_{CTD}$ binding to ssDNA *in vitro*

To reveal the molecular basis of BRCA2-R2645G dysfunction, we next measured the DNA binding capacity of $BRCA2_{CTD}$-R2645G *in vitro* by Electrophoretic Mobility Shift Assay (EMSA). 5 minutes incubation of a ^{32}P-labeled 167 nt ssDNA with increasing concentrations of $BRCA2_{CTD}$-WT at 37°C, generated a slower mobility species corresponding to DNA–protein complexes. ssDNA binding activity reached ∼80% of ssDNA–protein complex at the maximum concentration used (7 μM) when run at 4°C. $BRCA2_{CTD}$-R2520L yielded a similar fraction of ssDNA-protein complexes. Strikingly, $BRCA2_{CTD}$-R2645G showed higher apparent affinity (K_d 3.9 versus 7.5 μM) than the $BRCA2_{CTD}$-WT or the mutant $BRCA2_{CTD}$-R2520L (Figure 3A, Table 2). Interestingly, R2645G gave rise to two types of protein-DNA complexes based on their mobility.

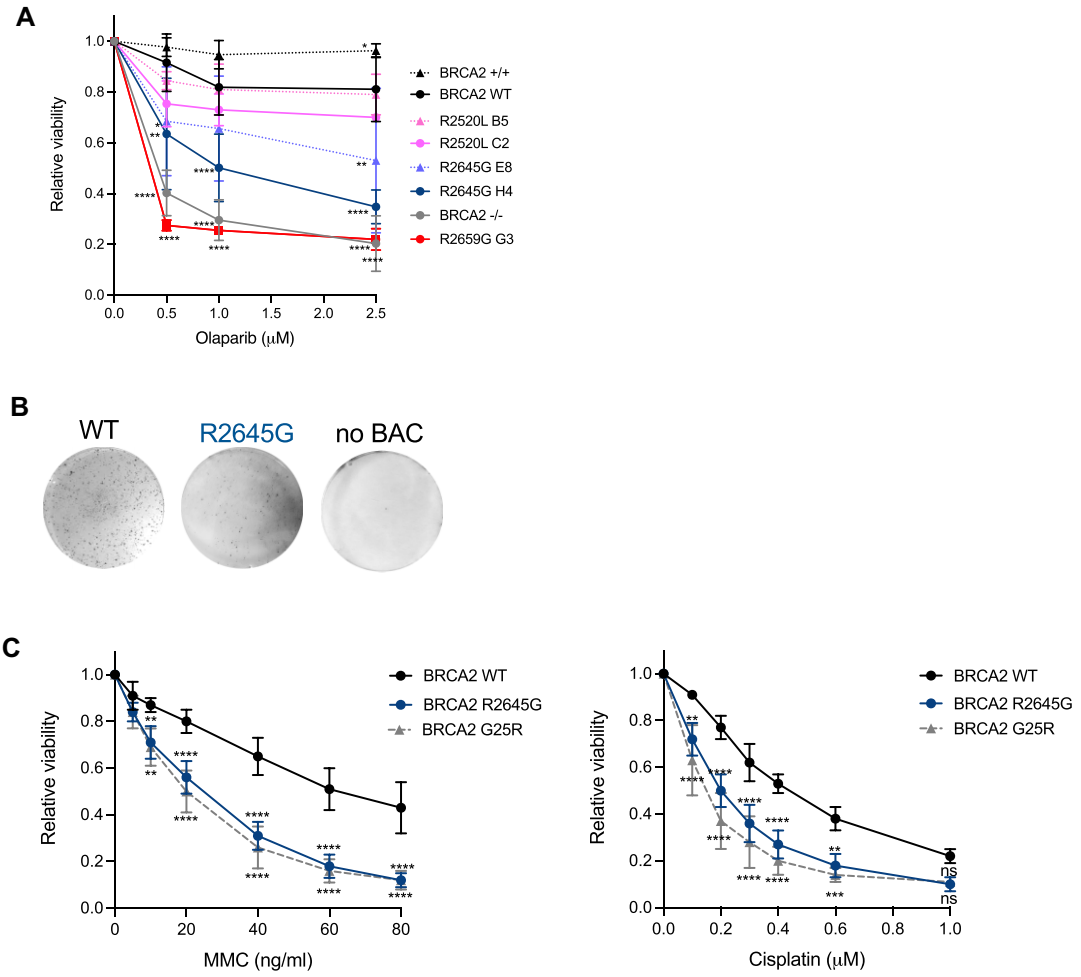

Figure 2. The *BRCA2 R2645G* variant confers sensitivity to genotoxic agents. (**A**) Quantification of the relative cell viability monitored by MTT assay in human DLD1 cells upon treatment with increasing doses of the PARP inhibitor Olaparib, as indicated. The data represent the mean ± SD of 2–6 independent experiments. A two-way ANOVA test with Dunnett's multiple comparisons test was used to calculate the statistical significance of differences (*P*-values show significant differences compared to the BRCA2 WT clone). Only significant values are shown. (**B**) Representative images of methylene blue staining of HAT-resistant colonies of mES cells expressing no BAC, BRCA2 WT or the BRCA2 R2645G variant. (**C**) Quantification of the relative cell viability monitored by an MTT assay upon treatment with increasing doses of the MMC (left) or cisplatin (right), as indicated. The data represent the mean ± SD of three independent experiments. A two-way ANOVA test with Dunnett's multiple comparisons test was used to calculate the statistical significance of differences (the *P*-values show significant differences compared to the BRCA2 WT clone). Only significant values are shown.

DSS1 has been described as a competitor for DNA binding (25) or promoting the monomeric form of BRCA2 which in turn would favor DNA binding (10). To test whether DSS1 would compete with the $BRCA2_{CTD}$-DNA complex, we used purified DSS1 from bacteria and performed an EMSA with ssDNA as in Figure 3A this time incubating increasing concentrations of $BRCA2_{CTD}$ WT or $BRCA2_{CTD}$-R2645G (0.5–7 μM) with or without DSS1 (5 μM) for 15 min at 37°C before adding the DNA. Under these conditions, the apparent affinity was slightly higher for both proteins but still, R2645G showed higher affinity than $BRCA2_{CTD}$-WT, K_d = 3.4 μM and 5.7 μM, respectively (Figure 3B and Table 2), consistent with the previous results (Figure 3A). Addition of DSS1 did not substantially affect the $BRCA2_{CTD}$-ssDNA interaction nor did it affect the interaction of $BRCA2_{CTD}$-R2645G with DNA (Figure 3B, Table 2).

Together, these results demonstrate that variant R2645G increases ssDNA binding affinity or DNA binding stability of BRCA2 whereas R2520L supports ssDNA binding as the $BRCA2_{CTD}$ WT. Moreover, an excess of DSS1 does not prevent DNA binding by the $BRCA2_{CTD}$.

BRCA2 R2645G does not impair BRCA2 self-interacting complex

BRCA2 forms dimers/multimers *in vitro* and these multimers have also been observed in cells (10,16,26). Based on previous models (10), an increase in DNA binding as observed in $BRCA2_{CTD}$-R2645G, is expected to favor the monomeric form of BRCA2. To verify the self-interacting complex in our cell system, we co-transfected human embryonic kidney HEK293T cells with MBP-BRCA2-RFP and GFP-MBP-BRCA2, or with GFP-MBP-NLS (nuclear localization signal) as a control. We then used a GFP-trap to pulldown MBP-BRCA2-RFP. Our results indicated that GFP-MBP-BRCA2 formed a complex with MBP-BRCA2-RFP, whereas this was not the case for the control. Moreover, the complex was not sensitive to benzonase suggesting the interaction is not mediated by DNA/RNA (Supplementary Figure S3A). We then performed the same experiment with BRCA2 R2645G. However, the level of RFP-BRCA2 WT pulldown by the mutated protein did not significantly differ from the pulldown by BRCA2 WT suggesting that BRCA2 R2645G can form a

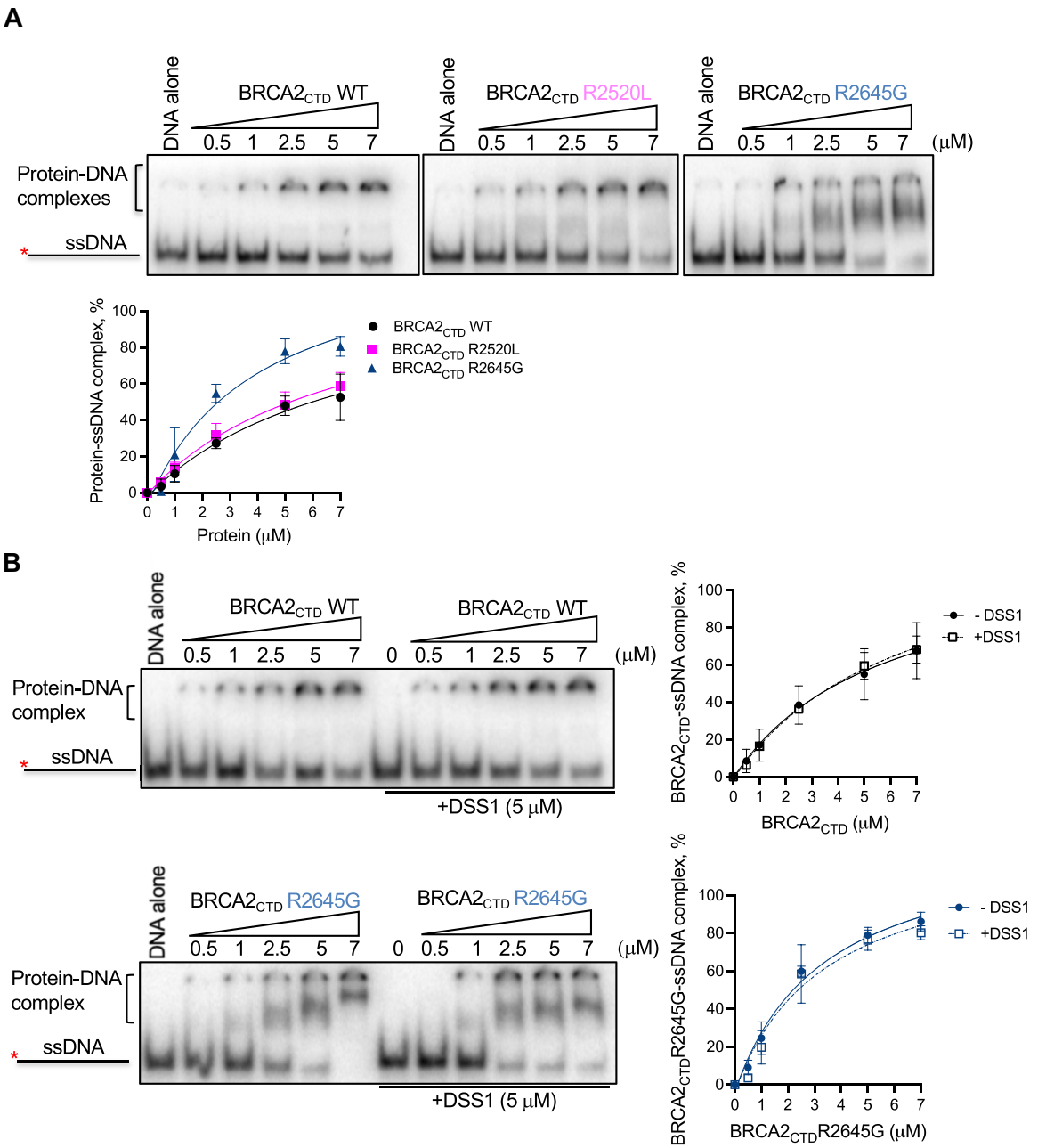

Figure 3. The *BRCA2 R2645G* variant enhances $BRCA2_{CTD}$ binding to ssDNA *in vitro*. (**A**) (Top) Representative EMSA and (bottom) quantification comparing the ssDNA (167 nt) binding activity of $BRCA2_{CTD}$ WT, $BRCA2_{CTD}$ R2520L and $BRCA2_{CTD}$ R2645G at increasing concentrations, as indicated. The data represent the mean from three independent experiments and it was fitted to a single-site binding curve. Error bars, SD. (**B**) (Left) Representative EMSA showing $BRCA2_{CTD}$ WT binding to ssDNA (167nt) at the specified concentrations after incubation with 5 μM DSS1, as indicated, for 15 min at 37°C. (Right) Quantification of (B). The data represent the mean from three independent experiments and it was fitted to a single-site binding curve. Error bars, SD.

self-interacting complex with BRCA2 WT in cells (Supplementary Figure S3B).

Cells expressing BRCA2 R2645G exhibit hyper-recombination phenotype

Given the enhanced ssDNA binding activity of $BRCA2_{CTD}$ R2645G, we reasoned that this variant might increase HR levels in cells. Using the stable clones expressing the full-length protein BRCA2 WT or the three variants, we performed a cell-based HR assay. In this assay, co-transfection of

Table 2. The apparent affinity of $BRCA2_{CTD}$-ssDNA or the indicated variants in the presence or absence of DSS1

Name	K_d (μM)	K_d -DSS1	K_d + DSS1
$BRCA2_{CTD}$ WT	7.5 ± 4.2	5.7 ± 3.6	6.7 ± 2.0
$BRCA2_{CTD}$ R2520L	7.0 ± 2.9	ND	ND
$BRCA2_{CTD}$ R2645G	3.9 ± 1.5	3.4 ± 0.8	3.4 ± 1.3

The apparent dissociation constant (K_d app ± SD) for $BRCA2_{CTD}$ binding was obtained from fitting the EMSA experiments shown in Figure 3A and B (15 min incubation with storage buffer of with DSS1 at 37°C before the addition of DNA) to a one-site binding curve.

two site-specific transcription-activator-like effector nuclease (TALENs) plasmids, along with a promoter-less mCherry plasmid containing homology arms for the AAVS1 locus results in a single DSB in the AAVS1 endogenous locus. Only when the DSB is repaired by HR do the cells express a mCherry fluorescent protein that can be quantified by flow cytometry (18). As expected, ∼11% of BRCA2 WT cells were mCherry+. In contrast, BRCA2 deficient cells (BRCA2$^{-/-}$) showed an average of 4% of mCherry+ cells, nearly matching the background levels in the absence of TALENs (2.6%). The HR capacity of the two stable clones bearing R2520L was similar to the one of the cells expressing the BRCA2 WT clone (9% and 13%). Strikingly, cells expressing the R2645G variant exhibited an increased HR activity (16% and 21% mCherry+ cells, respectively) compared to BRCA2 WT complemented cells (Figure 4A, Supplementary Figure S4A). This was not due to the differences in the expression levels as the clone that increased the activity the most (E8) showed equivalent BRCA2 protein levels as the BRCA2 WT clone (Supplementary Figure S4B).

Hyper-recombination may lead to chromosomal aberrations due to the possibility of pairing with homologous sequences that fuel genome instability (27). To explore this, we prepared chromosome spreads of DLD1 *BRCA2* deficient cells or bearing BRCA2 WT and BRCA2-R2645G left untreated or challenged with the DNA alkylating agent MMC (3 μM 1h). As expected, *BRCA2*$^{-/-}$ displayed increased chromosomal aberrations including radials, breaks, and fusions as compared to the BRCA2 WT cells after MMC treatment (Figure 4B). Interestingly, cells expressing BRCA2-R2645G did not significantly increase the number of total aberrations in MMC conditions, however, there was a consistent increase in chromatid gaps (Figure 4B), in agreement with the sensitivity to MMC observed in mES cells bearing this variant (Figure 2C).

Association of R2645G variant with breast, ovarian, and prostate cancer high-risk

To investigate the potential clinical relevance of the R2645G variant we collected three pedigrees carrying this variant. In them, several first relatives were affected with either breast, ovarian, or prostate cancer in addition to the index case (Figure 5A). Unfortunately, no DNA from relatives was available to perform co-segregation analysis, therefore an association of this variant to increased susceptibility to *BRCA2*-associated cancers will require further investigation.

Discussion

In this work, we investigated the potential impact of BRCA2 missense variants located in BRCA2$_{CTD}$ on DNA binding and DSS1 interaction to shed light on the role of these activities on the HR function of BRCA2. Unexpectedly, we report that R2645G, a variant recently classified as likely benign (19) and located at the interface with DSS1, increased the ssDNA binding capacity of the BRCA2$_{CTD}$ *in vitro* resulting in hyper-recombination in cells as measured by a cell-based HR reporter assay (18) and prompting chromosomal instability (Figure 5B). This instability instigates moderate to high sensitivity to different DNA damage-inducing agents like PARPi, alkylating agents (cisplatin), or crosslinking agents (MMC). To our knowledge, this is the first example of a *BRCA2* variant inducing a hyper-recombinant phenotype.

The effect on DNA binding of the variant R2645G was surprising considering the distance of R2645 to the putative DNA binding site inferred from the crystal structure of mouse Brca2$_{CTD}$ (PBD 1MJE) (5) and the human model derived from it (Figure 1A). However, the isolated HD and OB1 domain has been reported to bind DNA, although with weak affinity (5); therefore, it is possible that a structural change in the interface with DSS1 due to the mutation R2645G, reflected by the mild reduction of the thermal stability of the mutated BRCA2$_{CTD}$ (Table 1), facilitates binding of this variant to the DNA. It has been previously suggested that the acidic nature of DSS1 may expose the basic residues of the DSS1-binding groove in the HD and OB1 domains of BRCA2$_{CTD}$ (5,7), thus favoring the interaction with DNA. Thus, it is also possible that this modification influences the balance between DSS1- and DNA- binding.

According to current models, DSS1 regulates monomer-dimer species of BRCA2 which in turn, influence DNA binding. Therefore, we speculate that altering the contact with DSS1 would have an indirect effect on DNA binding through the change in the oligomeric form it produces. However, we could not detect a difference in the self-interaction of BRCA2 by pull-down in cells (Supplementary Figure S3B). Nonetheless, we cannot exclude a small reduction in the self-interaction of the protein which would not be detectable in our overexpression conditions.

In agreement with the role of human DSS1 in allowing DNA binding (10), rather than competing with it (25) we observed virtually no change in the affinity of BRCA2$_{CTD}$-WT- or BRCA2$_{CTD}$-R2645G-ssDNA complex when incubated with DSS1 (Figure 3B, Table 2). We did observe a slight increase in the apparent affinity of both the WT and the mutated form for DNA in this assay most likely due to the incubation of the protein at 37°C for 15 min before the addition of the DNA.

Remarkably, this work also reveals the destabilizing effect of the pathogenic variants BRCA2$_{CTD}$-I2627F and R3052W (Supplementary Figure S2C, Table 1) which could explain their severe phenotype in HR activity (6,28) despite their co-purification with DSS1 (Supplementary Figure S2A, B).

Our findings suggest that the activity of BRCA2 binding to DNA requires fine-tuning to keep HR under control, so that variants with altered DNA binding, either decreased or increased, such as R2645G, cause defective HR, and we propose that DSS1 contributes to the regulation of BRCA2 interaction with DNA.

A previous report described that Poly-ADP-Rybosylation (PARylation) of BRCA1 by PARP1 negatively modulates HR activity by decreasing BRCA1 avidity for DNA (29). They further showed that certain cancer-derived BRCA1-mutated cell lines are defective in BRCA1-PARylation and display a hyper-recombination phenotype. Although BRCA2 is not a target of PARylation, BRCA2$_{CTD}$ has been reported to directly bind PAR chains (30) which could be acting as a negative regulator of the BRCA2-ssDNA complex by direct competition in the cell. Whether the interaction with PAR chains is affected in BRCA2-R2645G or whether or not this interaction modulates DNA binding will require further investigation. Along the same lines, it is known that the control of HR through the dismantling of RAD51 filaments is critical to avoid pairing with homologous sequences outside the sister chromatid or prevent the formation of toxic recombination intermediates(31). Interestingly, the tumor-associated variant RAD51 G151D was shown to induce a hyper-recombinant phenotype

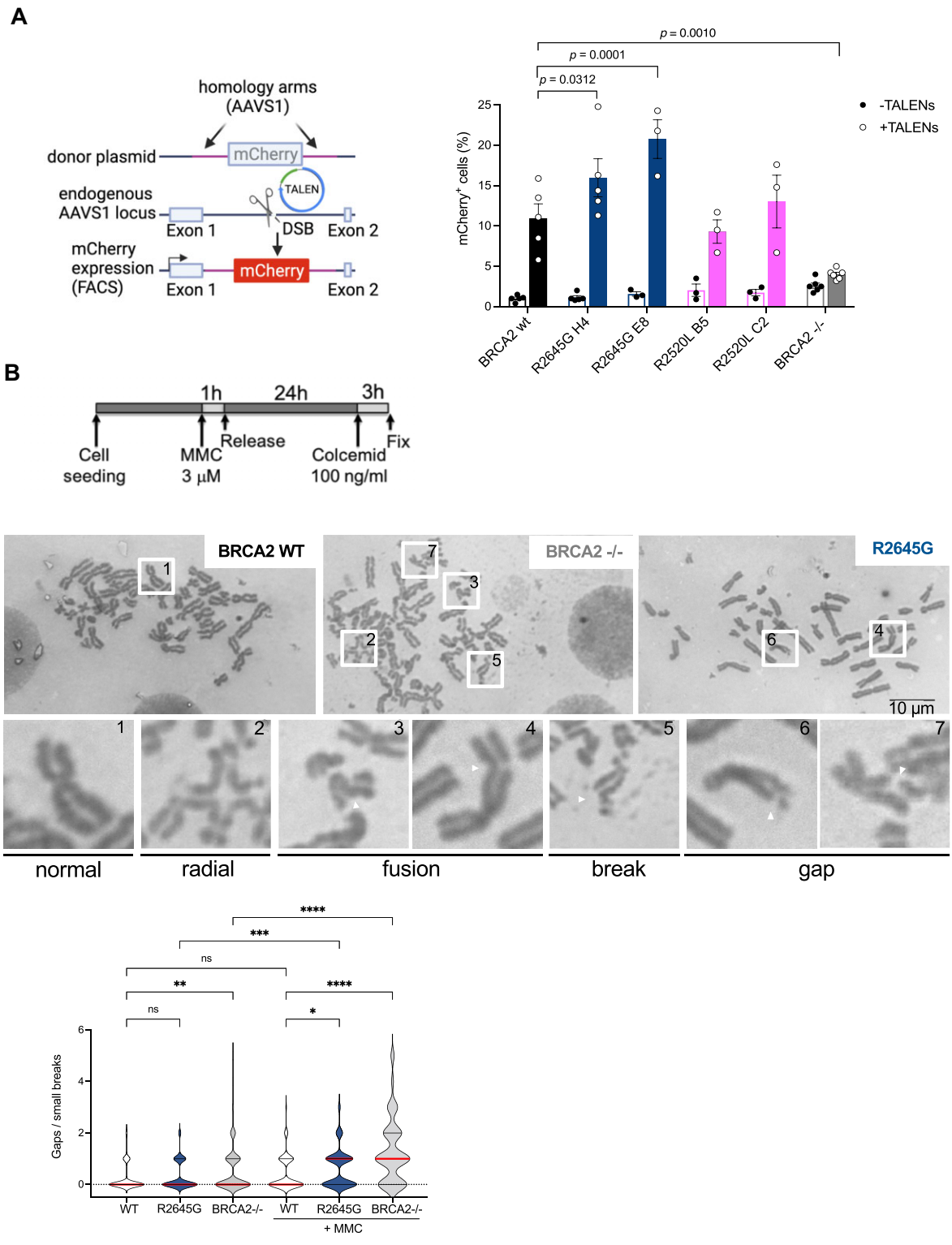

Figure 4. Human DLD1 expressing BRCA2 R2645G exhibit hyper-recombination. (**A**) (left) Scheme of the cell-based HR assay. (Right) Frequency of mCherry positive cells transfected with the promoter-less donor plasmid (AAVS1-2A-mCherry) without (−TALEN) (filled circles) or with (+TALEN) nucleases (open circles). The error bars represent the mean ± SEM of two to four independent experiments. Two-way ANOVA test with Dunnett's multiple comparisons test. The p-values show significant differences compared to the BRCA2 WT clone. (**B**) (top) Schematic representation of the experiment timing and the dose of MMC used to detect chromosomal aberrations and representative images of metaphase spreads of DLD1 BRCA2-deficient cells (BRCA2−/−) or BRCA2−/− cells stably expressing BRCA2 WT or BRCA2-R2645G (c. E8), as indicated, treated with 3 μM MMC for 1h. The type of chromosomal aberrations observed is indicated with numbers and magnified below. (Bottom). Quantification of chromosomal gaps/small breaks from the same cells either left untreated or upon treatment with MMC, as indicated. Data represent the median and 25% and 75% quartiles of three independent experiments where 50 metaphase spreads were analyzed in each experimental data set. Statistical difference was determined by the Kruskal-Wallis test followed by Dunn's multiple comparison test. ns, not significant, $*P < 0.05$, $**P < 0.01$, $***P < 0.001$, $****P < 0.0001$.

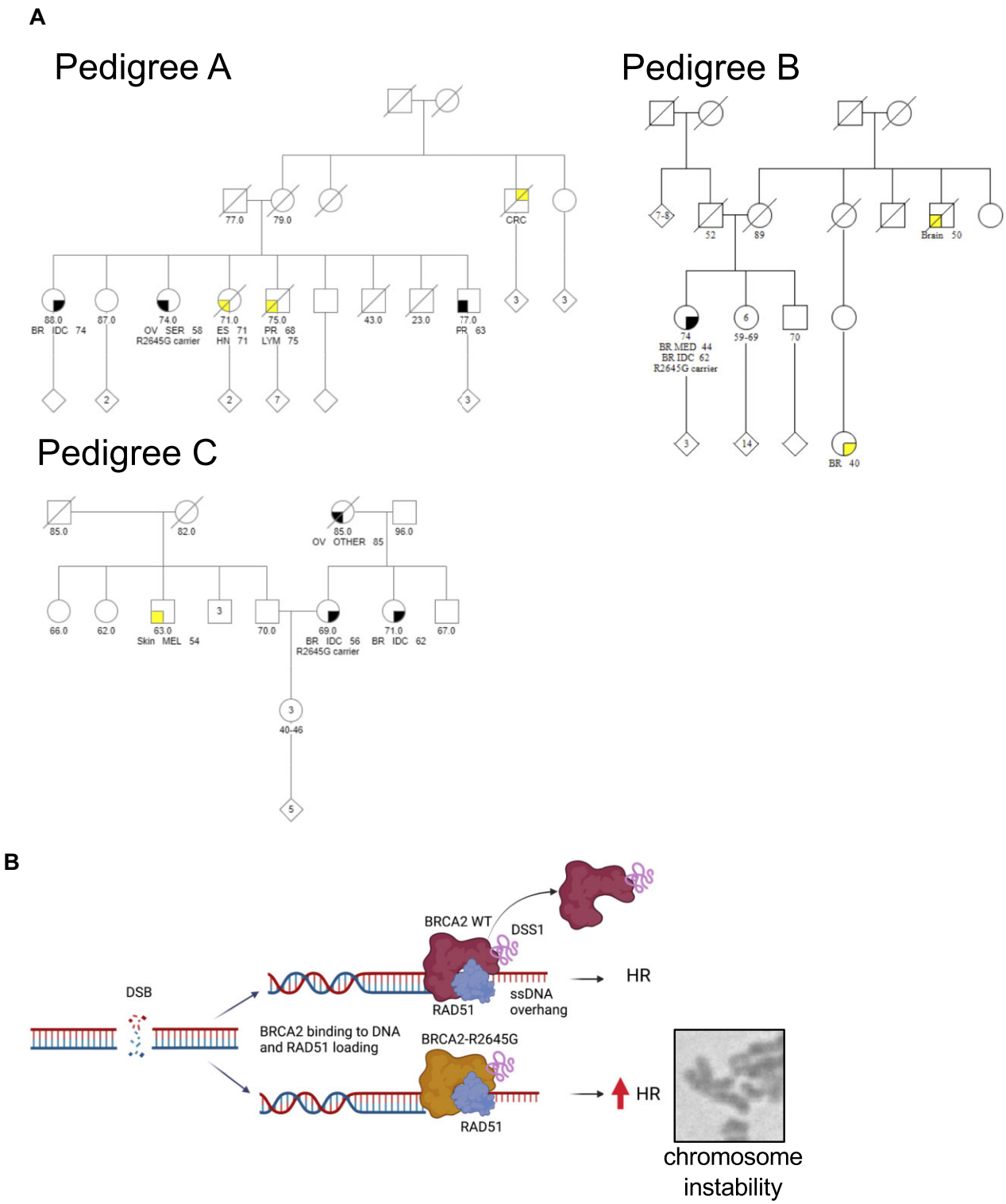

Figure 5. R2645G segregates with breast cancer in high-risk families. (**A**) Individual pedigrees (A–C) containing the R2645G variant. A number inside an icon indicates the number of individuals. Black filed portions in icons denote report-confirmed cancers, and yellow portions denote unconfirmed cancers. The patient's current age or decease age is indicated under individuals' icons. Below is the cancer location, histology (where available), and age at diagnosis: BR – breast cancer, Brain – brain tumor, CRC – colorectal cancer, ES – esophageal cancer, HN – head and neck cancer, OV – ovarian cancer, PR – Prostate cancer, Skin – skin cancer; IDC – invasive ductal, MED – medullary, MEL – melanoma, OTHER – other histology (non-serous), SER – serous. Variant carriers are indicated (only index cases were tested). (**B**) Working model: Based on previous literature, the active form of BRCA2 would be a monomer that is favored by its interaction with DSS1(10). Upon a DSB, BRCA2 WT bound to DSS1 locates and loads RAD51 at the ssDNA/dsDNA junction. This allows the formation of a nucleoprotein filament of RAD51 on ssDNA, the limiting step to promote HR. The variant BRCA2-R2645G makes more stable or higher affinity complexes with ssDNA than the BRCA2 WT protein (which might eventually be released from the DNA); this results in hyper-recombination activity in cells expressing this variant. As a consequence, cells expressing BRCA2-R2645G display a higher frequency of chromosomal instability in the form of chromatid gaps when challenged with MMC and higher sensitivity to different genotoxic agents including PARPi, MMC and cisplatin. Figure created with BioRender.com.

(32) Thus, the regulation of BRCA2-DNA interaction could be acting as an additional means to control HR.

The phenotype of cells bearing R2645G both in human DLD1 and mES cells suggests that this variant is hypomorphic in cells, which might have clinical consequences for individuals carrying this variant. However, a recent article classified R2645G as likely benign, based on a multifactorial likelihood model (19). This model was designed to assess high penetrance variants, so it could misleadingly classify a hypomorphic or moderate risk variant as VUS or (likely) benign. Considering all the available data, we would nowadays classify this variant as of uncertain significance given that (i) although rare, it is not absent from population databases; (ii) it scores 0.634 in the widely recognized *in silico* meta-predictor REVEL, an intermediate value according to ClinGen thresholds (33) and (iii) the cell-based and *in vitro* assays presented here demonstrate an impact on function. Intriguingly, the defective mechanism appears to be different from most BRCA2 missense variants. Understanding the clinical implications for *BRCA2 R2645G* carriers will require an international effort to collect sufficient clinical data and undertake low-penetrance-adapted case-control, family history, or cosegregation studies.

Data availability

Authors declare that all relevant data are included in the paper and/or its supplementary information files. Correspondence and requests for materials should be addressed to A.C.

Supplementary data

Supplementary Data are available at NAR Online.

Acknowledgements

We thank all members of Carreira lab for their input on this manuscript. We thank Stacey Stauffer and Eileen Southon for their help with the ES cell work. We are grateful to Charlene Lasgi from the Flow Cytometry platform of Institut Curie, Orsay.

Author contributions: L.A.-A, A.P., Y.D., D.P., J. K. S., A.E., D.V., C.M., S. M., E.J., S.C., A. C, designed the experiments; L.A.-A, A.P., Y.D., D.P, J. K. S., A.E., D.V., C.M., S. M., A.C-P., N.N., V. B., P.L., I. D., F.Q. performed the experiments; all authors analyzed the data; A.C. wrote the manuscript with input from all the authors and A.C., D.S.L., S.C., S.Z-J., C. L., E.J., and S.K.S. supervised the research. Funding Acquisition, A.C., S.Z-J., C. L., S.C., E. R., D.S.L.

Funding

Agence National de Recherche [ANR-17-CE12-0016]; Institut National du Cancer [INCa-DGOS_8706]; Matmut; Agencia Española de Investigacion (MCIN/AEI) [PID2020-115977RB-I00 to A.C.]; L.A.-A. was funded by an FPI Fellowship from Agencia Española de Investigacion (MCIN/AEI) [PID2020-115977RBI00]; Fondation ARC pour la Recherche sur le cancer and the French Ministry of Education (to D.V.); Fondation pour la Recherche Medicale (FRM) (to I.D.). Funding for open access charge: Institut Curie (Matmut).

Conflict of interest statement

None declared.

References

1. Carreira,A., Hilario,J., Amitani,I., Baskin,R.J., Shivji,M.K.K., Venkitaraman,A.R. and Kowalczykowski,S.C. (2009) The BRC repeats of BRCA2 modulate the DNA-binding selectivity of RAD51. *Cell*, **136**, 1032–1043.
2. Jensen,R.B., Carreira,A. and Kowalczykowski,S.C. (2010) Purified human BRCA2 stimulates RAD51-mediated recombination. *Nature*, **467**, 678–683.
3. Patel,K.J., Yu,V.P., Lee,H., Corcoran,A., Thistlethwaite,F.C., Evans,M.J., Colledge,W.H., Friedman,L.S., Ponder,B.A. and Venkitaraman,A.R. (1998) Involvement of Brca2 in DNA repair. *Mol. Cell*, **1**, 347–357.
4. Julien,M., Ghouil,R., Petitalot,A., Caputo,S.M., Carreira,A. and Zinn-Justin,S. (2021) Intrinsic disorder and phosphorylation in BRCA2 facilitate tight regulation of multiple conserved binding events. *Biomol*, **11**, 1060.
5. Yang,H., Jeffrey,P.D., Miller,J., Kinnucan,E., Sun,Y., Thoma,N.H., Zheng,N., Chen,P.-L., Lee,W.-H. and Pavletich,N.P. (2002) BRCA2 function in DNA binding and recombination from a BRCA2-DSS1-ssDNA structure. *Science*, **297**, 1837–1848.
6. Guidugli,L., Pankratz,V.S., Singh,N., Thompson,J., Erding,C.A., Engel,C., Schmutzler,R., Domchek,S., Nathanson,K., Radice,P., *et al.* (2013) A classification model for BRCA2 DNA binding domain missense variants based on homology-directed repair activity. *Cancer Res.*, **73**, 265–275.
7. Gudmundsdottir,K., Lord,C.J., Witt,E., Tutt,A.N.J. and Ashworth,A. (2004) DSS1 is required for RAD51 focus formation and genomic stability in mammalian cells. *EMBO Rep.*, **5**, 989–993.
8. Li,J., Zou,C., Bai,Y., Wazer,D.E., Band,V. and Gao,Q. (2005) DSS1 is required for the stability of BRCA2. *Oncogene*, **25**, 1186–1194.
9. Zhou,Q., Kojic,M., Cao,Z., Lisby,M., Mazloum,N.A. and Holloman,W.K. (2007) Dss1 interaction with Brh2 as a regulatory mechanism for recombinational repair. *Mol. Cell. Biol.*, **27**, 2512–2526.
10. Le,H.P., Ma,X., Vaquero,J., Brinkmeyer,M., Guo,F., Heyer,W.-D. and Liu,J. (2020) DSS1 and ssDNA regulate oligomerization of BRCA2. *Nucleic Acids Res.*, **45**, 4507–4516.
11. Zhou,Q., Mazloum,N., Mao,N., Kojic,M. and Holloman,W.K. (2009) Dss1 regulates interaction of Brh2 with DNA. *Biochemistry*, **48**, 11929–11938.
12. Zhao,W., Vaithiyalingam,S., Filippo,J.S., Maranon,D.G., Jimenez-Sainz,J., Fontenay,G.V., Kwon,Y., Leung,S.G., Lu,L., Jensen,R.B., *et al.* (2015) Promotion of BRCA2-dependent homologous recombination by DSS1 via RPA targeting and DNA mimicry. *Mol. Cell*, **59**, 176–187.
13. Nicolai,C.v., Ehlen,A., Martin,C., Zhang,X. and Carreira,A. (2016) A second DNA binding site in human BRCA2 promotes homologous recombination. *Nat. Commun.*, **7**, 12813.
14. Kwon,Y., Rösner,H., Zhao,W., Selemenakis,P., He,Z., Kawale,A.S., Katz,J.N., Rogers,C.M., Neal,F.E., Shabestari,A.B., *et al.* (2023) DNA binding and RAD51 engagement by the BRCA2 C-terminus orchestrate DNA repair and replication fork preservation. *Nat. Commun.*, **14**, 432.
15. Lee,M., Shorthouse,D., Mahen,R., Hall,B.A. and Venkitaraman,A.R. (2021) Cancer-causing BRCA2 missense mutations disrupt an intracellular protein assembly mechanism to disable genome maintenance. *Nucleic Acids Res.*, **49**, 5588–5604.
16. Shahid,T., Soroka,J., Kong,E., Malivert,L., McIlwraith,M.J., Pape,T., West,S.C. and Zhang,X. (2014) Structure and mechanism of action of the BRCA2 breast cancer tumor suppressor. *Nat. Struct. Mol. Biol.*, **21**, 962–968.
17. Jeyasekharan,A.D., Liu,Y., Hattori,H., Pisupati,V., Jonsdottir,A.B., Rajendra,E., Lee,M., Sundaramoorthy,E., Schlachter,S.,

Kaminski,C.F., *et al.* (2013) A cancer-associated BRCA2 mutation reveals masked nuclear export signals controlling localization. *Nat. Struct. Mol. Biol.*, **20**, 1191–1198.
18. Vugic,D., Ehlen,A. and Carreira,A. (2021) Monitoring homologous recombination activity in human cells. *Methods Mol. Biol.*, **2153**, 115–126.
19. Caputo,S.M., Golmard,L., Léone,M., Damiola,F., Guillaud-Bataille,M., Revillion,F., Rouleau,E., Derive,N., Buisson,A., Basset,N., *et al.* (2021) Classification of 101 BRCA1 and BRCA2 variants of uncertain significance by cosegregation study: a powerful approach. *Am J Hum Genetics*, **108**, 1907–1923.
20. Hucl,T., Rago,C., Gallmeier,E., Brody,J.R., Gorospe,M. and Kern,S.E. (2008) A syngeneic variance library for functional annotation of human variation: application to BRCA2. *Cancer Res.*, **68**, 5023–5030.
21. Lord,C.J. and Ashworth,A. (2017) PARP inhibitors: synthetic lethality in the clinic. *Science*, **355**, 1152–1158.
22. Bryant,H.E., Schultz,N., Thomas,H.D., Parker,K.M., Flower,D., Lopez,E., Kyle,S., Meuth,M., Curtin,N.J. and Helleday,T. (2005) Specific killing of BRCA2-deficient tumours with inhibitors of poly(ADP-ribose) polymerase. *Nature*, **434**, 913–917.
23. Kuznetsov,S.G., Liu,P. and Sharan,S.K. (2008) Mouse embryonic stem cell-based functional assay to evaluate mutations in BRCA2. *Nat. Med.*, **14**, 875–881.
24. Biswas,K., Das,R., Eggington,J.M., Qiao,H., North,S.L., Stauffer,S., Burkett,S.S., Martin,B.K., Southon,E., Sizemore,S.C., *et al.* (2012) Functional evaluation of BRCA2 variants mapping to the PALB2-binding and C-terminal DNA-binding domains using a mouse ES cell-based assay. *Hum. Mol. Genet.*, **21**, 3993–4006.
25. Zhou,Q., Kojic,M. and Holloman,W.K. (2012) Dss1 release activates DNA binding potential in Brh2. *Biochemistry*, **51**, 9137–9146.
26. Sidhu,A., Grosbart,M., Sánchez,H., Verhagen,B., Zon,N.L.L.v., Ristic,D., Rossum-Fikkert,S.E.v. and Wyman,C. (2020) Conformational flexibility and oligomerization of BRCA2 regions induced by RAD51 interaction. *Nucleic Acids Res.*, **48**, 9649–9659.
27. Malkova,A. and Haber,J.E. (2012) Mutations arising during repair of chromosome breaks. *Annu. Rev. Genet.*, **46**, 455–473.
28. Shimelis,H., Mesman,R.L.S., Nicolai,C., Ehlen,A., Guidugli,L., Martin,C., Calléja,F.M.G.R., Meeks,H., Hallberg,E., Hinton,J., *et al.* (2017) BRCA2 hypomorphic missense variants confer moderate risks of breast cancer. *Cancer Res.*, **77**, 2789–2799.
29. Hu,Y., Petit,S.A., Ficarro,S.B., Toomire,K.J., Xie,A., Lim,E., Cao,S.A., Park,E., Eck,M.J., Scully,R., *et al.* (2014) PARP1-driven poly-ADP-ribosylation regulates BRCA1 function in homologous recombination-mediated DNA repair. *Cancer Discov.*, **4**, 1430–1447.
30. Zhang,F., Shi,J., Bian,C. and Yu,X. (2015) Poly(ADP-Ribose) mediates the BRCA2-dependent early DNA damage response. *CellReports*, **13**, 678–689.
31. Krejci,L., Altmannova,V., Spirek,M. and Zhao,X. (2012) Homologous recombination and its regulation. *Nucleic Acids Res.*, **40**, 5795–5818.
32. Marsden,C.G., Jensen,R.B., Zagelbaum,J., Rothenberg,E., Morrical,S.W., Wallace,S.S. and Sweasy,J.B. (2016) The tumor-associated variant RAD51 G151D induces a hyper-recombination phenotype. *PLos Genet.*, **12**, e1006208.
33. Pejaver,V., Byrne,A.B., Feng,B.-J., Pagel,K.A., Mooney,S.D., Karchin,R., O'Donnell-Luria,A., Harrison,S.M., Tavtigian,S.V., Greenblatt,M.S., *et al.* (2022) Calibration of computational tools for missense variant pathogenicity classification and ClinGen recommendations for PP3/BP4 criteria. *Am. J. Hum. Genet.*, **109**, 2163–2177.
34. Warming,S., Costantino,N., Court,D.L., Jenkins,N.A. and Copeland,N.G. (2005) Simple and highly efficient BAC recombineering using galK selection. *Nucleic Acids Res.*, **33**, e36.
35. Plumb,J.A., Milroy,R. and Kaye,S.B. (1989) Effects of the pH dependence of 3-(4,5-dimethylthiazol-2-yl)-2,5-diphenyl-tetrazolium bromide-formazan absorption on chemosensitivity determined by a novel tetrazolium-based assay. *Cancer Res.*, **49**, 4435–4440.

Received: August 8, 2023. **Revised:** November 30, 2023. **Editorial Decision:** December 10, 2023. **Accepted:** December 12, 2023